Force-Based Interaction for Distributed Precision Assembly

Richard T. DeLuca

CMU-RI-TR-00-29

Submitted to the Department of Robotics
In Partial Fulfillment of the Requirements for the Degree of
Master of Science in Robotics

The Robotics Institute
Carnegie Mellon University
Pittsburgh, PA

December, 2000

This work was supported in part by the NSF through grants DMI-9523156 and DMI-9900165.

Abstract

This thesis documents the efforts to incorporate force sensing into the *minifactory* environment. The minifactory is a high-precision assembly system that makes use of low DOF robots to cooperatively perform higher DOF tasks. Minifactory targets the assembly of small mechatronic devices, many of which require high tolerance vertical insertion tasks. Force sensing provides a means for instantiating cooperative behaviors between robotic agents to perform such insertion tasks. Force sensing is a natural medium in which position and force information is acquired, allowing the compliancy needed to perform the task to be built into the behaviors of the robots performing the task. Integrating force sensing into the minifactory required that a custom force sensor be developed as well as control and communication systems to coordinate the action of two minifactory agents. Test results are presented from experiments in which two high-precision 2-DOF robotic agents cooperatively perform contact and "peg-in-hole" tasks. These results document the first experimental confirmation of high-bandwidth ($> 100\,\mathrm{Hz}$) coordination between agents within the minifactory system.

Thesis supervisor: Dr. Ralph Hollis
Principal Research Scientist, Robotics Institute

Acknowledgments

I am extremely fortunate to be one of the first full-time Masters students of the Robotics Institute. There are a few people I would like to thank for making this possible. I would like to thank Dr. Ralph Hollis, my advisor and reason for being at the RI. I am grateful for his guidance and the opportunity he gave me to work in the Microdynamic Systems Laboratory. The experience surpassed any of my expectations. Besides the tremendous lab space and equipment, the people with whom I've had an opportunity to work are brilliant. Dr. Al Rizzi became a mentor to me. His advice was paramount to my success. Previous work by Jay Gowdy, Arthur Quaid, Zack Butler, Michael Chen, Ben Brown, Patrick Muir, Shinji Kume, and Jimmy Ma made my work possible. I would also like to thank my family and friends for always supporting me.

Contents

List of Figures

List of Tables

1 Introduction

Advances in technology are creating numerous driving forces that require high-tech manufacturing companies to look towards automation for solutions. Competitive markets place pressure on companies to focus on reducing manufacturing costs and time-to-market. However, as the product life cycle decreases, the cost of setting up an assembly line becomes a more significant portion of the production cost [1]. Advances in technology have also resulted in product miniaturization, requiring assembly tasks that are very difficult or impossible for manual labor to accomplish. There is a need for an assembly environment which is flexible enough to adapt to short product life cycles and accommodate products that require precision assembly.

Robotics and automation potentially provide an answer to these problems. Whereas automation systems currently exist to perform manufacturing tasks, they are often very difficult and expensive to configure, calibrate, and modify. These systems generally lack the flexibility to easily reconfigure and incorporate new machinery into the assembly line.

1.1 The Agile Assembly Architecture and Minifactory

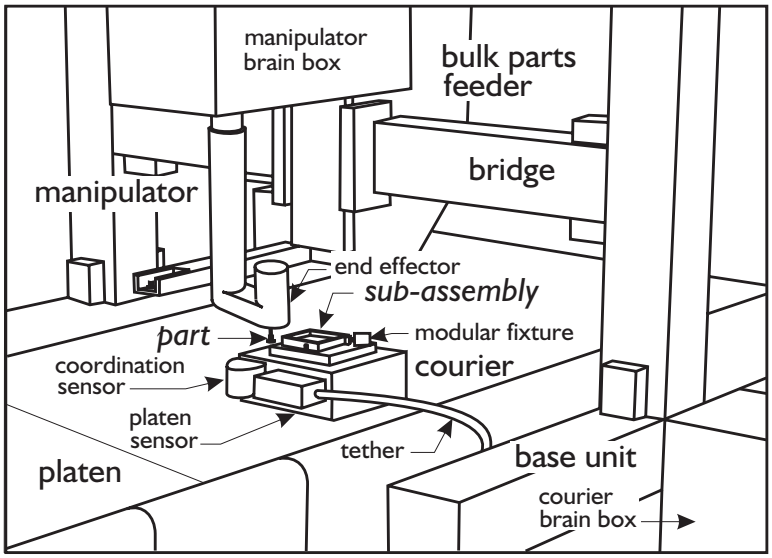

Figure 1: The major components of a minifactory system.

At the Microdynamic Systems Laboratory[1] we are developing a high-precision assembly system, called minifactory, that is modular, rapidly reconfigurable, and self-calibrating. The minifactory project is a physical instantiation of a much broader philosophy for precision assembly systems: an Architecture for Agile Assembly (AAA). The motivation of AAA and the minifactory is to create a new standard for autonomous assembly systems. The minifactory relies on a collection of low degree-of-freedom (DOF) robots capable of cooperatively performing assembly tasks (See Figure 1). The use of modular and distributed components allows minifactory to be extremely flexible in factory design, and reconfiguration [2]. Critical to

[1] See `http://www.cs.cmu.edu/~msl`.

cooperative interaction between robotic agents and high-precision assembly is the inclusion of suitable sensing capabilities. Recently our group reported success with the application of frame-rate visual sensing for inter-agent coordination [3, 4]. The work presented in this thesis complements that earlier work and discusses the application of precision force-based interaction between robotic agents of the minifactory.

1.2 Minifactory Infrastructure

Minifactory comprises 2-DOF robotic devices (termed agents) which are physically, computationally, and algorithmically modular. There are two classes of robotic agents used to perform the experiments presented in this thesis, couriers and overhead manipulators. Used cooperatively, these agents can perform 4-DOF tasks. To facilitate such cooperation the minifactory relies on a network designed to handle high-bandwidth communication.

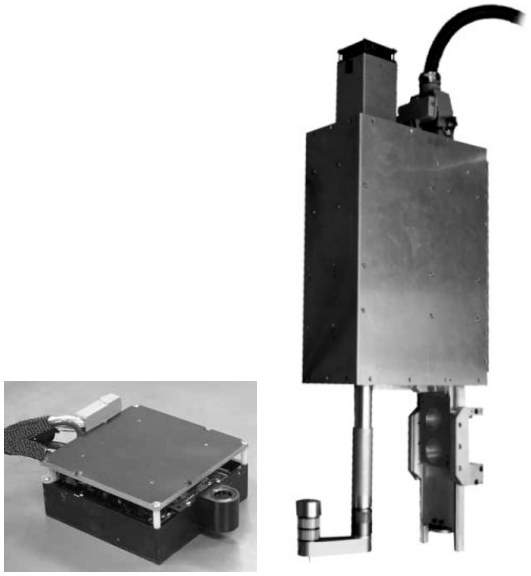

(a) (b)

Figure 2: Minifactory Agents: Courier (a) and Overhead Manipulator (b).

Courier robots (Figure 2(a)), which operate in the plane of the factory floor, serve as the factory's conveyor system, shuttling subassemblies to various parts of the factory. Couriers provide translation in x and y and limited rotation. The courier agent is a modified planar linear motor equipped with a magnetic sensor that can resolve position to $200\,\mathrm{nm}$ (1σ) [5]. The sensor allows the courier to operate in closed loop, providing improved position resolution, reduced power consumption, and dynamic manipulation capabilities [6]. The courier is also fitted with an optical sensor used to detect LED beacons mounted on overhead manipulators hanging on bridges above the couriers [7]. This functionality is used in factory calibration during which couriers explore the factory [8].

Overhead manipulator agents (Figure 2(b)) operate above the factory floor and perform pick and place

operations. The two active DOFs for the overhead manipulator are z (translational) and θ (rotational). The manipulator has a range of $125\ \mathrm{mm}$ in z with a resolution of $2\ \mu\mathrm{m}$, and $\pm 270°$ range in θ with a resolution of $0.0005°$. To aid in pick and place operations our prototype manipulator is equipped with a frame grabber and camera system for visual servoing, and a multi-axis force sensor for force-based interaction (described in Section 2).

Vital to the operation of the minifactory is a robust inter-agent communication infrastructure. Minifactory has a global network and a high speed local network. The global network facilitates factory-wide communication using standard IP protocols over a 100 Mb Ethernet network. The local network, called AAA-Net, uses semi-custom network protocols over a 100 Mb Ethernet network, providing a means for agents to interactively perform high-bandwidth tasks [3, 9]. Section 3.2 details the use of the local network to facilitate high-bandwidth agent cooperation.

Agents run computer processes at two levels. The high-level processes consist of Python[2] scripts which are responsible for managing the semantics of factory operation and the associated discrete events. These higher-level processes typically communicate via the global network. Lower-level processes sequence and execute real-time control laws. These processes are written in C or C++ and if necessary communicate via the high-bandwidth AAA-Net.

1.3 Motivation for Force Based Interaction in the Minifactory

Following the AAA standard for robotic agents to be self-calibrating and tolerant of uncertainties in factory configuration, robotic agents designed for the minifactory must have suitable sensing capabilities. The most natural and informative sensing ability for tasks involving contact is force sensing.

Force sensing can provide solutions to a few common problems in autonomous assembly. Systems without force sensing must rely on pure kinematic descriptions of the robot and its environment. This requires tedious and costly measurements and calibrations to be made. The addition of a force sensor permits a robot to detect collisions with its environment and adjust its models to fit the real environment and choose an appropriate behavior. Another issue occurs when dealing with fragile parts: a robot without force sensing can not accurately measure the applied forces, risking damaging the part. Force sensing provides rich information that make high-tolerance insertion procedures, normally impossible with other sensing modalities, realizable. Most notably in the case of the minifactory, force sensor information is used as a means of instantiating cooperative behaviors between robotic agents.

The use of force sensors to enable the performance of contact tasks is a well studied topic in robotics literature. The work presented here builds directly on many earlier efforts – most notably the work by Mason [11], Craig and Raibert [12], Hogan [13], Anderson and Spong [14], Khatib [15], and Siciliano [16]. This thesis details the effort to incorporate these ideas and the appropriate force sensing capabilities to perform a “peg-in-hole” task using a flexible distributed automated assembly system.

[2] Python is a portable object oriented scripting language extendible by C or C++ code [10].

2 Force Sensing Hardware

2.1 Motivation for New Hardware

There is a wide selection of commercially available force sensors to choose from, but none that meet the varied design requirements that the minifactory application presents. High precision assembly with small parts requires small force resolution. In the spirit of AAA, modularity and efficient integration are important. Vision and gripping modalities were already in place on prototype end effectors and a force sensor was sought to neatly fit into the system, allowing gripping devices to be easily interchanged.

2.2 Force Sensor Design

The kinematics of many assembly applications under consideration for minifactory involve vertical insertion operations using a single point vacuum gripper. This type of operation requires that only the applied force and two lateral moments be measured. Other important design considerations were sensitivity, integrability, low hysteresis, and range. A respectable minimum sensitivity for the force sensor was determined to be $0.1\ \mathrm{N}$ with a range of several Newtons. In terms of integrability, it was sought to make the force sensor's z-sensitive axis coaxial with the vacuum gripping tube and the camera. It is important that the force sensor be designed such that it does not occlude the camera. Figure 3 shows an exploded assembly drawing of the end effector with vision, force sensing, and gripping devices compactly integrated.

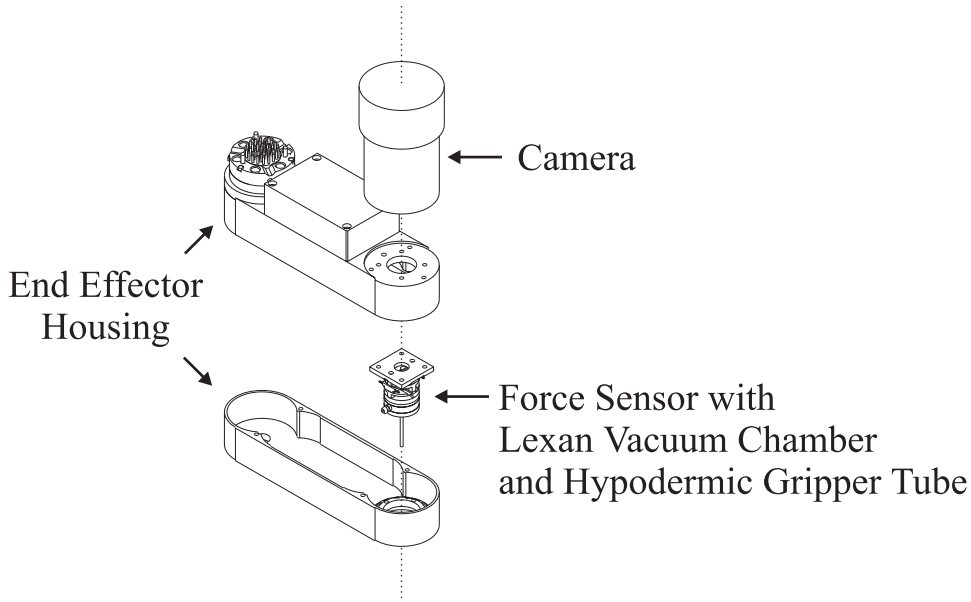

Figure 3: An exploded drawing of the end effector assembly.

Several sensing technologies were considered during the design process, including semiconductor and foil strain gauges, as well as capacitive, inductive, piezoelectric, and optical elements. Strain gauges have

(a) (b) (c) (d)

Figure 4: 3-Axis force sensor: (a) drawing of the mechanical flexure, (b) exploded assembly drawing of the flexure and single-axis load cells, (c) photograph of the flexure with clear lexan vacuum chamber and one load cell, (d) flexure with four load cells in place.

been used effectively in many robotic force sensing applications but suffer from temperature dependence, fragility, and difficulties in installation. Piezoelectirc devices provide high sensitivity and signal to noise ratios, but are difficult to manufacture. Piezoelectric crystals used passively can only provide dynamic force information and are susceptible to drift for constant force measurements. The complexity of designing an active piezoelectric device removed it from consideration. Capacitive, inductive, and optical elements can all be used to measure small deflections, making them possible candidates for use in a force sensor; however, these sensing modalities are either bulky, require complicated electronics, or flexures that contain elements with hysteresis[17].

The final design utilizes a set of commercial single-axis load cells incorporated into a mechanical flexure. Cooper Instruments[3] manufactures the LPM 562, a single-axis piezoresitive load cell, see Figure 4(c). Incorporated into a mechanical flexure, these load cells were used to form a 3-axis force sensor that is inexpensive, thermally insensitive, and easily manufactured.

The 3-axis force sensor design can be seen in Figure 4. An applied force and torque are transmitted to the load cells through a flexure. Assuming small deflections, linear analysis of the flexure yields a model relating applied forces and moments to load cell readings. The model was formed using beam theory to describe the deflections of the thin sections of the flexure, treating the rest of the flexure as rigid. The load cells were modeled as linear springs using the full scale load and deflection specifications provided by Cooper Instruments. The model takes the form

$$\begin{bmatrix} V_1 \\ V_2 \\ V_3 \\ V_4 \end{bmatrix} = \underbrace{\begin{bmatrix} \frac{\alpha_1}{\beta_1} & \frac{\epsilon_1}{\beta_1} & 0 \\ \frac{\alpha_2}{\beta_2} & \frac{\epsilon_2}{\beta_2} & 0 \\ \frac{\eta_1}{\delta_1} & 0 & \frac{\zeta_1}{\delta_1} \\ \frac{\eta_2}{\delta_2} & 0 & \frac{\zeta_2}{\delta_2} \end{bmatrix}}_{C} \begin{bmatrix} F \\ M_x \\ M_y \end{bmatrix}, \tag{1}$$

where F, M_x, and M_y represent the applied force and moments respectively, while V_i represents the

[3] See `http://www.cooperinstruments.com/index.html`.

measured load cell voltages. Ideally, if the load cells are symmetrically arranged within the flexure it will be the case that $\alpha_1 = \alpha_2$, $\beta_1 = \beta_2$, $\epsilon_1 = -\epsilon_2$, $\eta_1 = \eta_2$, $\delta_1 = \delta_2$, and $\zeta_1 = -\zeta_2$, leaving only four unknown parameters required to characterize the sensor.

Finite element analysis was used to validate the assumptions made in the development of the above model. ProMechanica was used to perform the analysis. Deflection results were of the same order of magnitude as found in the above model, validating the treatment of the thin sections of the flexure as cantilever beams.

2.3 Force Sensor Analysis

Once fabricated, the force sensor was calibrated to validate the model and determine the appropriate transformation matrix to convert measured load cell voltages to applied force and torques for the device as built. The experiment performed to accomplish this involved mounting a flat plate to the force sensor and applying a range of loads to the plate at 49 points evenly spaced over the entire plate. Measurements from each load cell were sampled at $1\,\mathrm{kHz}$ and averaged over a period of $3\,\mathrm{s}$ to remove sensor and electrical noise.

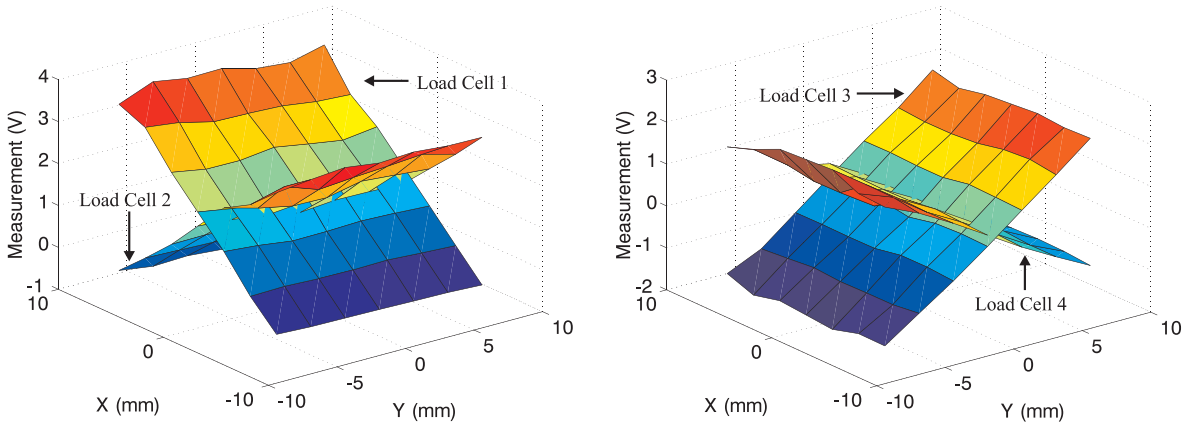

(a) (b)

Figure 5: Load cell output for a $2\,\mathrm{N}$ force applied at 49 points on a flat plate attached to the flexure. Output from load cells 1 and 2 (a). Output from load cells 3 and 4 (b).

Figure 5 shows the output from the load cells given a $2\,\mathrm{N}$ input force over the surface of the plate mounted to the force sensor. The results are as one might expect; the output from each load cell forms a sloped plane. The flexure is designed such that the output from the load cell pairs should be sensitive in only one axis of applied torque. As the applied force is moved further from the center of the flexure (increase in torque) the output should increase linearly. Each load cell pair should then form two planes that intersect at the center of the flexure. This is the case as shown in the Figure 5. Figure 6 shows output from individual load cells for multiple input forces over the plate's surface. Notice that load cell pairs are sensitive to changes in torque in only one axis for which the directions corresponding to each pair are

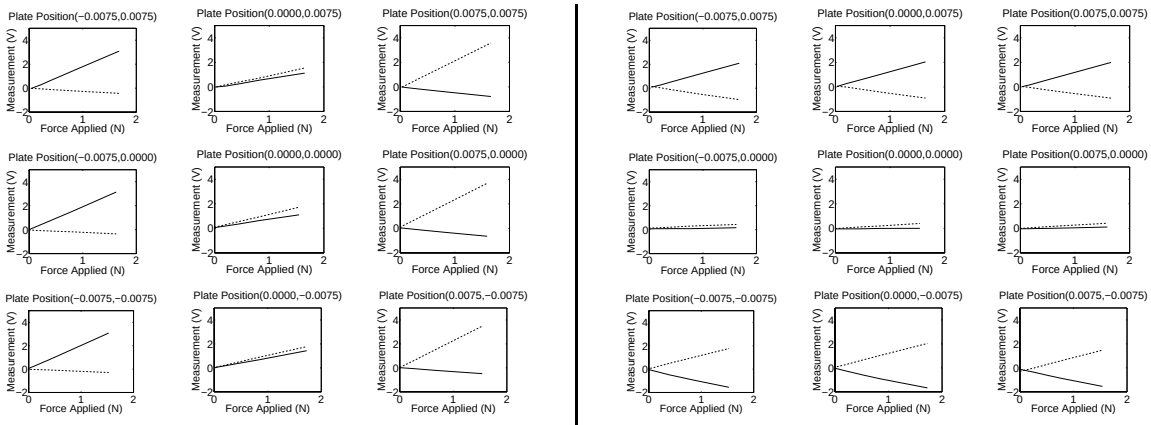

Figure 6: Load cell outputs for forces applied to 9 points on a flat plate attached to the flexure. Output from load cells 1 and 2 (a). Output from load cells 3 and 4 (b).

orthogonal.

Linear regression was performed on the outputs of the individual load cells to produce an estimate, $\hat{C}$, of the calibration matrix C,

$$\hat{C} = \begin{bmatrix} 0.594 & -121 & -9.66 \\ 0.791 & 129 & -5.31 \\ 0.0804 & -3.44 & 120 \\ 0.184 & -9.56 & -82.1 \end{bmatrix}.$$

The occurrence of non-zero elements and the lack of symmetry can be attributed to fabrication and assembly inaccuracies including load cell placement and machining tolerances. In particular, lateral displacement of the load cells was not considered in the idealized model. Based on this calibration of the sensor and observed noise properties of the sensing elements, this force sensor is capable of resolving forces down to roughly $24\ \mathrm{mN}$ (1σ) and torques of approximately $0.13\ \mathrm{mN \cdot m}$ (1σ).

2.4 Force Sensor Integration

Steps were taken in the areas of mechanical, electrical, and software integration to successfully incorporate the force sensor into the overhead manipulator. The single-axis load cells produce an electrical signal of $0 - 60\ \mathrm{mV}$ proportional to the applied load. The load cells only operate in compression and produce $0\ \mathrm{V}$ unloaded. The load cells are preloaded in the flexure such that they nominally produce a $30\ \mathrm{mV}$ signal when the flexure is unloaded. An instrumentation amplifier is used with a gain of 100 to increase the load cells' output to $0 - 6\ \mathrm{V}$. An anti-aliasing filter board was developed using a Sallen-Key low-pass filter with a cutoff frequency placed at $100\ \mathrm{Hz}$. This serves to eliminate high frequency noise from the load cells and limit the bandwidth of the sensor to $100\ \mathrm{Hz}$ which is reasonable for use with an A/D converter that is sampling at $2\ \mathrm{kHz}$. The filter board also applies a gain of 1.5 so that the output from the force sensor makes

better use of the entire $10\ \mathrm{V}$ input range of the A/D converter. The filter board is located in the end effector near the load cells. Placed in the overhead manipulator, high frequency noise is picked up in wires that run through the manipulator arm close to motors. A digital filter implemented in software was designed to reduce the effect of noise on the force sensor channels. A second order digital Butterworth filter with a corner frequency at $100\ \mathrm{Hz}$ was chosen for the task. Voltage measurements from the load cells are then converted to force and torque measurements through matrix G, which is the psuedo inverse of matrix $\hat{C}$. The resulting force sensitivity achieved by the sensor placed in the overhead manipulator is approximately $78\ \mathrm{mN}$ (1σ) in z and $0.6\ \mathrm{mN \cdot m}$ (1σ) in x/y.

3 System Integration

With hardware in place, the objective is to use the hardware in an intelligent manner to perform a "peg-in-hole" task. In order to effectively implement control, the dynamics of the system must be understood. Once a generalized model of the system has been developed, we wish to instantiate the control system in a manner that efficiently utilizes inter-agent communication by using algorithmically simple control schemes.

3.1 System Modeling

The model developed considers both the courier and overhead manipulator. The courier can be modeled as a mass with essentially ideal actuators in the x and y directions. This is the direct result of the simple actuation of the courier and the frictionless air bearing that supports the courier [18, 19]. The overhead manipulator's θ axis is directly driven, resulting in negligible friction and an equally simple model. The z axis is driven by a ball screw so a friction term was included to account for the effects of friction in that axis. Thus, the dynamic model of the system takes the form

$$\underbrace{\begin{bmatrix} M_z & 0 & 0 & 0 \\ 0 & M_\theta & 0 & 0 \\ 0 & 0 & M_x & 0 \\ 0 & 0 & 0 & M_y \end{bmatrix}}_{M_a} \underbrace{\begin{bmatrix} \ddot{z} \\ \ddot{\theta} \\ \ddot{x} \\ \ddot{y} \end{bmatrix}}_{\ddot{q}} + \underbrace{\begin{bmatrix} B_z & 0 & 0 & 0 \\ 0 & 0 & 0 & 0 \\ 0 & 0 & 0 & 0 \\ 0 & 0 & 0 & 0 \end{bmatrix}}_{B_a} \underbrace{\begin{bmatrix} \dot{z} \\ \dot{\theta} \\ \dot{x} \\ \dot{y} \end{bmatrix}}_{\dot{q}} + \underbrace{\begin{bmatrix} f_z sgn(\dot{z}) \\ 0 \\ 0 \\ 0 \end{bmatrix}}_{f(\dot{q})} = \underbrace{\begin{bmatrix} \tau_z \\ \tau_\theta \\ \tau_x \\ \tau_y \end{bmatrix}}_{\tau_a} - \underbrace{\begin{bmatrix} F_z \\ rF_\theta \\ F_x \\ F_y \end{bmatrix}}_{F_e}, \quad (2)$$

where q represents the generalized configuration of the system; M_a and B_a describe the overhead manipulator's and courier's mass and damping parameters; $f(\dot{q})$ contains the friction terms; τ_a represents the applied actuator forces; and F_e is the applied environmental forces.

3.2 Controller Architecture

The control methodologies described here most closely resemble the class of impedance controllers originally proposed by Hogan [13]. Impedance control provides a convenient way to interact stably with the environment. Under impedance control, not only is the desired motion of the system dictated, but also the

controller encapsulates how the system should interact with the environment. Impedance control converts the system to a form that naturally performs the task. In this case, given a desired mass (M_d), stiffness (K_d), damping (B_d), and force (F_d) the desired system behavior is given by

$$M_d\ddot{q} + K_d(q - q_0) + B_d\dot{q} + G_i \int_0^t (F_e - F_d)d\tau = F_e, \tag{3}$$

where the system is made to behave like a mass attached to a spring and damper about a nominal target position q_0, with the added integral term driving the system to the desired contact forces F_d. F_e are the applied environmental forces. It is this last term that will be measured by the force sensor mounted on the manipulator's end effector described in Section 2.

Given the system model and desired impedance, applying inverse dynamics yields a control law of the form

$$\tau_a = M_a M_d^{-1}\left[F_e + K_d(q_0 - q) - B_d\dot{q} + G_i \int_0^t (F_e - F_d)d\tau\right] + B_a\dot{q} + f(\dot{q}) + F_e. \tag{4}$$

This control law is implemented separately on the two agents, with each agent responsible for its actuated degrees of freedom. There is a moderate amount of freedom in how the control law is implemented. By choosing to only allow diagonal matrices for M_d, K_d, B_d, and G_i this control policy is completely diagonal, which implies that the only information that must be shared between the agents is the sensed environmental forces[4]. This requires that information only flow in one direction; from the manipulator to the courier.

To simplify the amount of infrastructure that is implemented on each agent, the courier control law was enhanced to allow the manipulator to command velocities and controller mode. The velocity commands and controller mode information allow the manipulator agent to command four different behaviors from the courier agent. The velocity command is accomplished by the modification of the damping term from $B_d\dot{q}$ to $B_d(\dot{q} - \dot{q}_0)$, where $\dot{q}_0$ is the desired velocity. In addition, the desired position, q_0, is moved appropriately at each time step to achieve the desired velocity. The controller mode simply determines if the integral term in the courier control law is active or zeroed. If both the velocity command and integral term are zeroed, the courier behaves as the non-enhanced system would; like a mass attached to a spring and damper about the target position. If just a velocity is commanded the courier will behave as if the target position is moved at the commanded velocity. If the integral term is activated with a zero velocity command, the courier will seek to apply the desired force on the gripper. Lastly, if both a velocity is commanded and the integral term is activated then the system will behave as if it is under hybrid position/force control as proposed by Craig and Raibet [12].

Impedance control is one of many control laws that is used to accomplish high level tasks in the minifactory. Minifactory makes use of a hybrid control strategy, of the form described in [20], that activates underlying continuous control policies based on the current state of the machine by decomposing the state space into overlapping regions and parameterizing controllers associated with each region. A *predicate* is defined as the boolean function associated with a specific controller that returns true if the system is within the bounded region associated with the controller. A controller will only activate if its predicate evaluates

[4] These are the interaction forces between the two agents.

to true. A prioritized list of controller and predicate pairs is maintained to determine which controller should be active.

Consider a simple motion in which the courier will move to a position and then maintain that position. To accomplish this, a PD controller is added to a priority queue. This PD controller has a small region around the goal position in which the controller will activate. A velocity controller that has a larger activation region is added to the queue with a lower priority than the PD controller. This controller scheme is designed to use the velocity controller to move the courier to the desired position at which point the PD controller's predicate will evaluate to true, activating the PD controller which maintains the desired position.

In addition to the impedance controller, which is responsible for handling contact tasks, there are a few other controllers that are used to setup and protect the system during the experiments described in Section 4. Velocity controllers are used to perform the gross movements of the robots. Controllers that are responsible for the system's actions near the velocity controllers' goal, such as an impedance controller, are added to the controller priority queue first and with higher priority. For instance, in the contact experiments an impedance controller is added to a priority queue on the manipulator with a predicate that has a small region in position near the contact surface. A velocity controller that will move the manipulator near the surface is then added to the queue with a lower priority than the impedance controller. As a safety precaution during each experiment a velocity controller is added with the highest priority to the queue that will move the robots into safe positions when the force sensor experiences large forces.

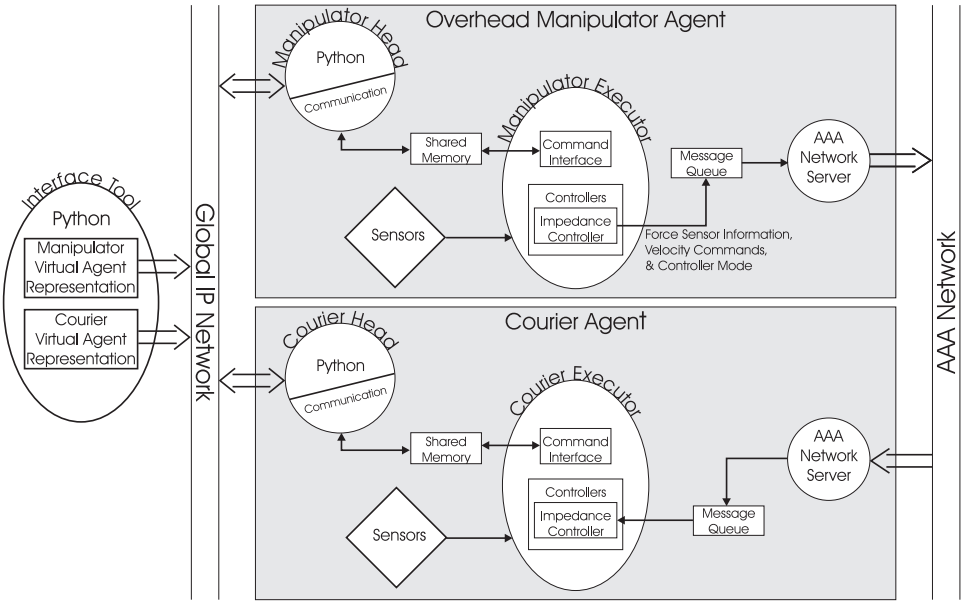

Figure 7: The communications infrastructure used for force-based interaction.

The communication infrastructure, briefly described in Section 1.2, is critical to implementing the above control law among distributed agents. Figure 7 shows the communication infrastructure needed for

cooperative force-based interaction. The top portion of this figure represents processes running on the overhead manipulator while processes running on the courier are shown in the lower portion. Circular and oval shapes represent individual processes while diamonds represent hardware resources. The interface tool, shown on the left of Figure 7, down-loads high-level Python scripts to the agents. These scripts specify the types of controllers that run on each agent and the sequence in which they are instantiated [21]. The interface tool communicates with the respective agent heads through the global network. The agent heads run the scripted program for each agent provided by the interface tool and communicate directly with the executor processes. The executor processes are hard-coded repositories of real-time control strategies and provide management for the execution and sequencing of those strategies [3, 22, 23]. Inter-agent communication is handled by the AAA-Net. Specifically, messages are sent to the courier from the overhead manipulator at real-time rates ($> 500\,\mathrm{Hz}$) and contain force sensor information, velocity commands, and controller mode.

4 Experimental Tests and Results

The experiments described in this section were performed with the minifactory agents configured as shown in Figure 8. In these experiments the overhead manipulator performed contact tasks with a 0.813 mm (0.032 in.) diameter hypodermic tube attached to the force sensor on the end effector (see Figure 8(b) and 4(b)). Mounted on the courier is a plate containing several sets of holes 6.35 mm (0.25 in.) in depth and ranging in diameter from 2.54 mm (0.1 in.) to 0.838 mm (0.033 in.) (see Figure 8). Each hole has a $45°$ chamfer.

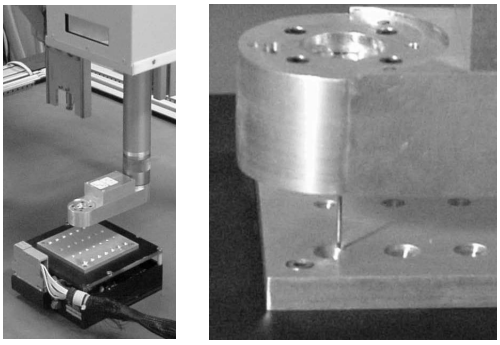

(a) (b)

Figure 8: (a) View of courier, configured for an insertion task, coordinating with an overhead manipulator. (b) Close up view of the manipulator's end effector preparing to insert a peg into a hole with an exaggerated chamfer.

Three basic contact tasks were performed to characterize the system performance: vertical contact, lateral contact, and peg-in-hole insertions (see Figure 9). In addition, experiments were performed to test the repeatability of the insertion task.

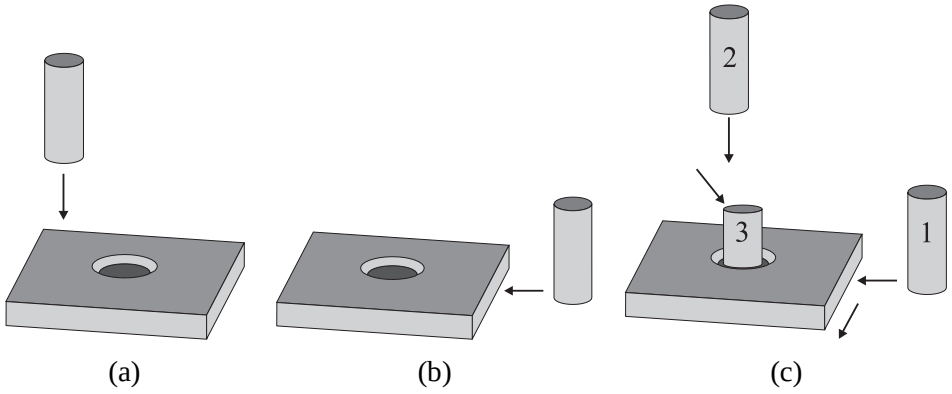

Figure 9: Graphic description of the three types of experiments performed: vertical contact (a), lateral contact (b), and peg-in-hole (c).

4.1 Vertical Contact

The vertical contact experiment involved the courier maintaining a fixed position while the overhead manipulator made contact and maintained a constant force with the plate. Specifically, the courier performed a move (under position control) to place it under the manipulator and held its position. Meanwhile, the manipulator found the top of the plate on the courier by executing a constant velocity, force-guarded move. With the exact position of the plate top registered, the manipulator servoed to a z position above the plate by a height equal to the depth of a hole. Once the tool tip has arrived at this position an impedance controller was automatically activated with the desired position located appropriately below the surface of the plate to obtain the desired contact force at equilibrium. For this experiment the desired z force was $-1\,\mathrm{N}$. Results from a typical experiment are shown in Figure 10. Note the slightly underdamped response of the z force and the steady state value of $-1\,\mathrm{N}$. The observed high frequency noise in the force information is attributed to unmodeled dynamics in the gripper tube. The settling time from impact is approximately $1\,\mathrm{s}$. Response rates faster than this were difficult to achieve without higher impact forces. Friction in z appears to be the limiting factor.

4.2 Lateral Contact

The goal of the lateral contact experiment was to position the tool tip below the plane of the top of the plate while the courier made contact and maintained a constant lateral force with the side of the plate. The top of the plate was located with a constant velocity, force-guarded move as in the vertical contact experiment. Controllers were then deployed to reposition the courier and bring it into lateral contact with the tool tip. When contact was made, the manipulator started an impedance controller that changed the mode of the courier controller and set the desired position for the courier to its position at the instance of contact. The desired contact force was set to $-0.4\,\mathrm{N}$ in y. Results of a typical experiment can be found in Figure 11. Notice that the force applied in the y direction reaches a steady state value of $-0.4\,\mathrm{N}$. A non-zero steady

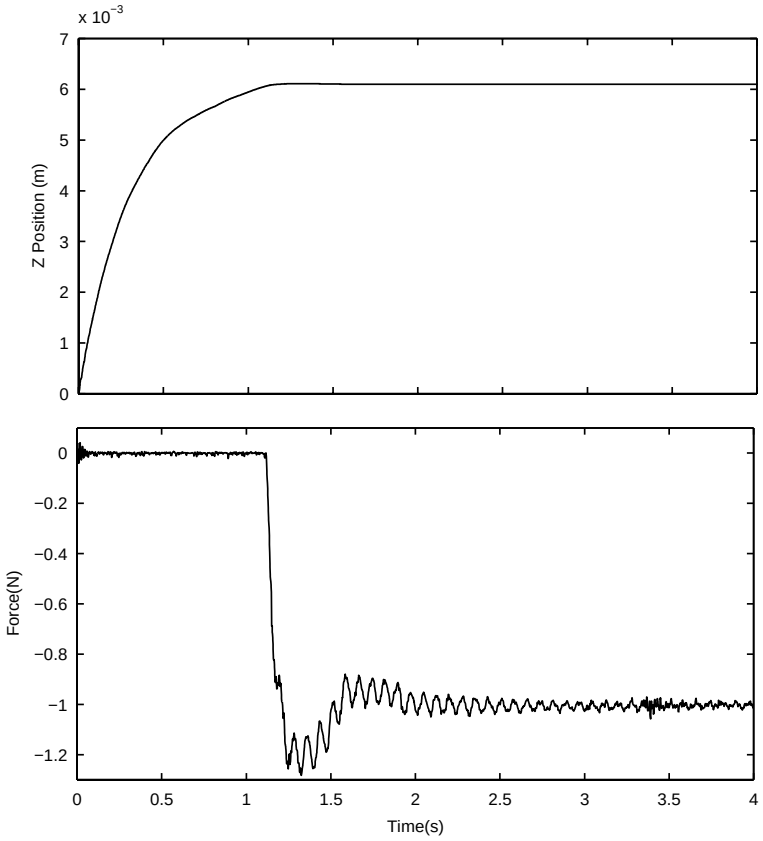

Figure 10: Position and force measurements during a vertical contact experiment.

state value for the x force can be attributed to small misalignments of the gripper tube, misalignments of the courier plate, or compliance in the manipulator's θ axis. The observed settling time is roughly 0.3 s. It is expected that faster settling times can be achieved for lateral contact in which the stiffness of the θ axis of the manipulator is increased.

4.3 Peg-In-Hole

The peg-in-hole experiment consisted of the courier bumping into and sliding along the manipulator gripper to register the plate corner and thus the entire plate geometry relative to the manipulator's tool tip. The initial bump and slide maneuver involved a hybrid position/force control sequence implemented through the use of the described impedance controllers. Once lateral contact was made, the manipulator commanded a velocity and a mode change to the courier such that it maintained a constant force and slid along the plate edge. When the courier lost contact with the gripper, the courier's position was noted immediately and the plate geometry was registered to determine the location of the hole in tool tip coordinates. The plate top location was then calibrated as described earlier and the courier was positioned so that the gripper was directly over a chamfer of a hole. The manipulator servoed to a position at the height of the

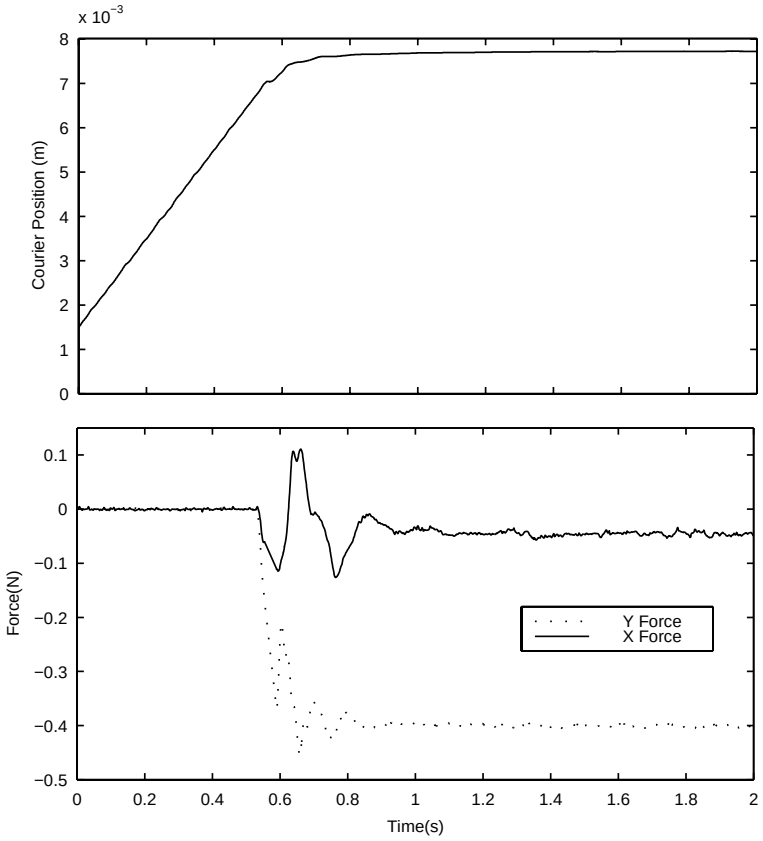

Figure 11: Position and force measurements during a lateral contact experiment.

plate top at which point an impedance controller activated with a desired position located at the center and appropriately below the bottom of the hole. The desired force was $-1\,\mathrm{N}$ in z and $0\,\mathrm{N}$ in x and y. Figure 12 shows typical results for this type of experiment. The insertion data presented is from an insertion performed on a hole with an exaggerated chamfer of diameter 6.35 mm (0.250 in.). The oversized chamfer was used to produce data with longer chamfer contact regions to aid in analysis. The exaggerated chamfer explains the lengthy duration of the insertion event. During chamfer contact it can seen that the tool tip follows the chamfer down into the hole as the courier moves in response to the x and y forces. It is expected that the change in x and y position during chamfer contact looks similiar to that of the change in z position. The relatively large change in x and y position at the beggining of the chamfer contact region, which occurs before contact is made, is due to the courier not having settled to the desired position before the experiment has begun. The settling time for the z force is comparable to that of the vertical contact experiment. Figure 13 shows the x,y trajectory of the tool tip during a typical insertion experiment. $\times$'s denote $0.1\,\mathrm{s}$ intervals. The even spacing of $\times$'s and the general straightness of the trajectory demonstrate the quality of the insertion procedure.

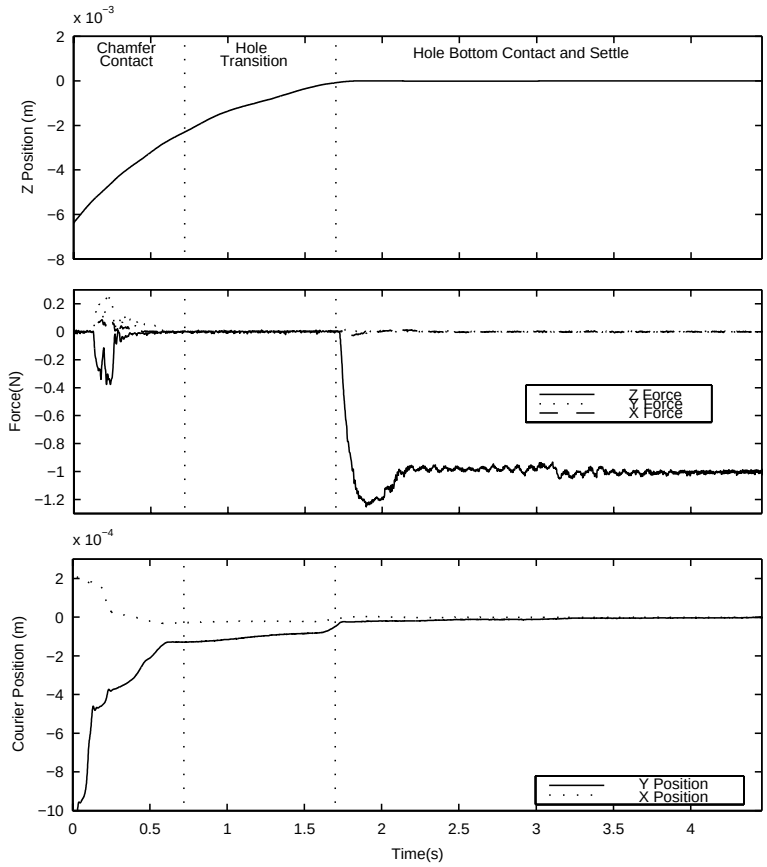

Figure 12: Overhead manipulator position, force, and courier position measurements during an insertion experiment.

4.4 Repeatability

Results are presented from two repeatability tests in which insertion tasks were initiated from uniformly distributed random points located above the chamfer. Repeatability was tested on a 1.016 mm (0.04 in.) hole with an exaggerated chamfer of diameter 6.35 mm (0.25 in.) and a 0.838 mm (0.033 in.) hole with a typical chamfer of diameter 1.52 mm (0.06 in.). Figure 14 shows the start and stop positions of the tool tip in configuration space from a typical experiment. Finish positions shown outside of the hole in Figure 14(b) are attributed to slight system miscalibration and our failure to account for rotation of the courier. Table 1 summarizes these experiments. The difference in average insertion time is due to differences in the size of the chamfers. It is important to note that although only 93% of the 0.838 mm (0.033 in.) hole insertion attempts made it successfully into the hole, 63 of the failed attempts are attributed to system level errors. In these cases, system level failures prevented the experiment from beginning. Discounting these failures, the overall success rate rises to 99.3% for the 0.838 mm (0.033 in.) holes. Vertical insertion with a round peg is a 5 DOF task. The courier and manipulator, cooperatively, can only control 3 of the 5 DOFs which presents a chance of wedging the peg. Smaller clearance holes present a higher chance of wedging, which

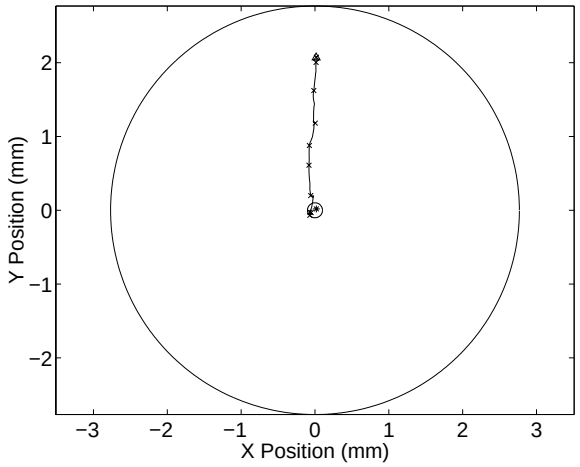

Figure 13: Tool tip trajectory plotted in configuration space during an insertion experiment. $0.1\,\mathrm{s}$ increments are noted with $\times$'s.

explains the larger RMS error in z force for the smaller clearance hole.

Hole Clearance	Ave. Time	Attempts	Success	RMS z Force Error
$0.2032\,\mathrm{mm}$ ($0.008\,\mathrm{in.}$)	$2.43\,\mathrm{s}$	1000	100%	$0.0663\,\mathrm{N}$
$0.0254\,\mathrm{mm}$ ($0.001\,\mathrm{in.}$)	$2.36\,\mathrm{s}$	1000	93%	$0.1091\,\mathrm{N}$

Table 1: Repeatability experiment results.

5 Summary and Conclusions

This thesis serves to document the successful integration of force sensing and distributed control policies into the minifactory for vertical insertion assembly tasks. The major accomplishments presented are the development of a custom 3-axis force sensor that combines compactness with suitable sensitivity for vertical insertion tasks; and the development of a distributed control policy that makes use of the inter-agent communications infrastructure already in place. In order to achieve success improvements were made to the minifactory infrastructure. Code was developed to perform high-speed logging of the overhead manipulator's internal state. It is important to note that the results presented are the first experimental confirmation of high-bandwidth ($> 100\,\mathrm{Hz}$) coordination between agents within the minifactory. The experimental results convincingly demonstrate the reliability of precision force-based insertion tasks performed by the minifactory.

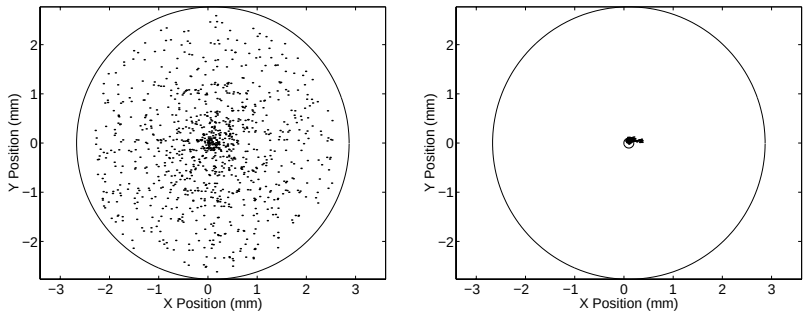

(a) (b)

Figure 14: Tool tip start (a) and finish (b) positions plotted in configuration space for repeatability test involving a hole with 0.02032 mm (0.008 in.) clearance.

6 Future Work

The first task for the immediate future is to use the infrastructure developed thus far to operate with real parts and subassemblies. The system is very close to being able to accomplish this as it is configured for the experiments in this thesis. Combining the 3-axis force sensor with a gripping modality on the manipulator that constrains the part from rotating may present problems. Experimentation with a square peg and square hole using the 3-axis force sensor would be interesting. Ideally at least a 4-axis force sensor would be needed for such a task.

Another task for the future is to explore other variations of the controller/communications architecture. The current control structure could be modified to include two way communication between agents, thereby allowing a non-diagonal control policy. I suspect this will allow the system to be tuned in a manner that produces higher performance (faster cycle times and smaller clearance holes). One such way to tune the system is to generate the desired spring and damping matrices of the impedance control such that the vitual springs and dampers are aligned with the slope of the chamfer as opposed to the generalized coordinates. This is effectively designing the system to avoid jamming on the chamfer.

Along these lines, another variation of the minifactory infrastrucutre would be the inclusion of a force sensor on the courier. In this configuration each agent would be responsible for sensing forces in the directions that they are capable of actuating in. This would eliminate the need for any force sensor information to be passed between agents.

Although the force sensor design presented is sufficient for many of the minifactory applications currently under consideration, redesign should be considered to allow for smaller force resolution and manufacturability. It would be interesting to experiment with the incorporation of different sensing modalities into the current flexure design.

Finally, there is a need to combine previous work with machine vision in our lab with the force-based interaction detailed here. One approach to this is to use the vision information to set the desired position for the impedance controller.

References

[1] P. M. Muir, J. Gowdy, and A. A. Rizzi, "Minifactory: A precision assembly system that adapts to the product life cycle," in *SPIE Symp. on Intelligent Systems and Advanced Manufacturing*, (Pittsburgh, PA), October 1997.

[2] A. A. Rizzi, J. Gowdy, and R. L. Hollis, "Agile Assembly Architecture: An agent-based approach to modular precision assembly systems," in *Proc. IEEE Int'l. Conf. on Robotics and Automation*, (Albuquerque, NM), April 1997.

[3] M. L. Chen, S. Kume, A. A. Rizzi, and R. L. Hollis, "Visually guided coordination for distributed precision assembly," in *Proc. IEEE Int'l Conf. on Robotics and Automation*, (San Francisco, CA), April 2000.

[4] M. L. Chen, "Visually guided coordination for distributed precision assembly," Master's thesis, Carnegie Mellon University, December 1999.

[5] Z. J. Butler, A. A. Rizzi, and R. L. Hollis, "Integrated precision 3-DOF position sensor for planar linear motors," in *Proc. IEEE Int'l. Conf. on Robotics and Automation*, (Lueven, Belgium), May 1998.

[6] A. E. Quaid, *A Planar Robot for High-Performance Manipulation*. PhD thesis, Carnegie Mellon University, 2000.

[7] W.-C. Ma, "Precision optical coordination sensor for cooperative 2-dof robots," Master's thesis, Carnegie Mellon University, 1998.

[8] Z. J. Butler, *Distributed Coverage of Rectilinear Environments*. PhD thesis, Carnegie Mellon University, 2000.

[9] S. Kume and A. A. Rizzi, "A high-performance network infrastructure and protocols for distributed automation," in *Proc. IEEE Int'l Conf. on Robotics and Automation*, 2001. (submitted).

[10] M. Lutz and D. Ascher, *Learning Python*. O'Reilly & Associates, Inc., 1999.

[11] M. T. Mason, "Compliance and force control for computer controlled manipulators," in *IEEE Transactions on Systems, Man, and Cybernetics*, pp. 418–432, June 1981.

[12] M. H. Raibert and J. J. Craig, "Hybrid position/force control of manipulators," in *Journal of Dynamic Systems, Measurement, and Control*, pp. 126–133, 1981.

[13] N. Hogan, "Impedance control: An approach to manipulation: Part i - theory, part ii - implementation, part iii - applications," in *Journal of Dynamic Systems, Measurement, and Control*, pp. 1–24, 1985.

[14] R. J. Anderson and M. W. Spong, "Hybrid impedance control of robotic manipulators," in *IEEE Journal of Robotics and Automation*, pp. 549–556, Oct 1988.

[15] O. Khatib, "A unified approach for motion and force control of robot manipulators: The operational space formulation," in *IEEE Journal of Robotics and Automation*, pp. 43–53, Feb 1987.

[16] S. Chiaverini, B. Siciliano, and L. Villani, "A survey of robot interaction control schemes with experimental comparison," in *IEEE Transactions on Mechatronics*, pp. 273–285, Sept 1999.

[17] J. Fraden, *Handbook of Modern Sensors: Physics, Designs, and Applications*. Woodbury, NY: American Institute of Physics, 2nd ed., 1997.

[18] A. E. Quaid and R. L. Hollis, "3-DOF closed-loop control for planar linear motors," in *Proc. IEEE Int'l Conf. on Robotics and Automation*, (Lueven, Belgium), May 1998.

[19] B. A. Sawyer, "Linear magnetic drive system." U. S. Patent 3,735,231, May 22 1973.

[20] A. A. Rizzi, "Hybrid control as a method for robot motion programming," in *IEEE Int'l. Conf. on Robotics and Automation*, (Leuven, Belgium), May 1998.

[21] J. Gowdy and Z. J. Butler, "An integrated interface tool for the Architecture for Agile Assembly," in *IEEE Int'l. Conf. on Robotics and Automation*, May 1999.

[22] J. Gowdy and A. A. Rizzi, "Programming in the Architecture for Agile Assembly," in *IEEE Int'l. Conf. on Robotics and Automation*, May 1999.

[23] A. A. Rizzi, J. Gowdy, and R. L. Hollis, "Distributed programming and coordination for agent-based modular automation," in *The Ninth International Symposium of Robotics Research*, (Snowbird, UT), October 1999.